Relating print velocity and extrusion characteristics of 3D-printable cementitious binders: Implications towards testing methods

Sooraj Nair[*], Subhashree Panda[†], Avinaya Tripathi[*], Narayanan Neithalath[‡]

Abstract

This study aims to relate print velocity to critical parameters extracted from a controlled ram extrusion test, towards a test method to expedite the selection of materials and process parameters for 3D-printing of cementitious materials. Higher print velocities, while aiding faster construction, results in a need for higher extrusion pressure, while lower velocities interfere with extrudate quality through effects such as water filtration. Steady-state pressures and dead-zone lengths corresponding to a chosen barrel-die geometry and print velocity are extracted from extrusion force-ram displacement relationships. The steady state pressure increases with print velocity, while the dead-zone length decreases. The deposition pressure between the nozzle exit and the print bed increases with increase in print velocity, and is proportional to the extrusion pressure. These results are used to define a range of desirable print velocities for the chosen geometry and the printer system, so that the extrusion pressure and dead-zone lengths are simultaneously optimized. The lower limit of the print velocity range, steady-state pressure, and dead-zone lengths are all lower when the material microstructural parameter (ratio of particle volume fraction to square of mean size) is higher, indicating the importance of appropriate material design in ensuring efficient 3D printing of cementitious binders.

Keywords: 3D printing; Extrusion; Cements; Print velocity; Steady-state pressure

* Graduate student, School of Sustainable Engineering and Built Environment, Arizona State University, Tempe AZ 85287
† Graduate student, School of Civil Engineering, University of Miami, Miami FL 33146
‡ Professor, School of Sustainable Engineering and Built Environment, Arizona State University, Tempe AZ 85287; Corresponding author: e-mail: Narayanan.Neithalath@asu.edu

1 Introduction

3D printing of concrete is an additive or digital manufacturing process that constructs a structure from a digital model. This method is gaining prominence due to its flexibility in construction of shapes that otherwise cannot be achieved using conventional formwork-based strategies [1,2]. Layered extrusion is one of the most common modes of concrete 3D printing and is currently the preferred method in the nascent field of 3D printing-based concrete construction [3–5]. The benefits of 3D printing of concrete include faster construction, minimization of construction-related errors, potential for shape-and-topology optimization, and efficient usage of materials. Currently, 3D printable binders are generally formulated based on trial-and-error to obtain desired fresh state rheological response (time-dependent yield stress and plastic viscosity), extrudability through the nozzle, and buildability (capability to maintain structural shape while resisting overburden pressures very soon after being laid) [6–9]. The complex early-age properties of cementitious binders and the difficulties in adequately measuring the ones relevant in extrusion-based 3D printing is a challenge that needs to be overcome.

Extrusion rheology is generally used to characterize concentrated suspensions of ceramics, polymers, and metals, the flow behavior of which involves internal shear deformations, shear hardening near the walls, wall slip effects, and barrel-to-die entry pressure losses [10]. Several models including the Bagley model and Benbow Bridgewater model are used to extract the entrance and wall slip stresses, slip effects, and material characteristics including extensional yield stress and die wall shear yield stress in such materials [11–13]. These approaches have been extended to cement-based materials as well, especially with the advent of extrusion-based concrete 3D printing. Liquid phase migration or dewatering can occur during extrusion of solid-water suspensions such as cement pastes due to weak particle-fluid interaction, especially under low velocities, leading to overpressure in extrusion [14–16]. The deformation zone geometry (barrel-to-die entry) and deadzone formation has been shown to influence the extrusion characteristics as well as the microstructure, and consequently the properties of the extrudate [17]. Several methods including vibration of the barrel, optimizing the extruder geometry, and modifying the particle characteristics (through changes in size distribution) or fluid features (e.g., viscosity) have been proposed to control pressure drop and mitigate liquid phase migration [18,19]. The effect of process conditions on the evolution of paste material deformation under extrusion is significant, and has been evaluated using analytical and numerical models [20–22]. Such experimental and analytical/numerical studies have demonstrated that a synergistic treatment of the materials and process conditions is critical in ensuring adequate extrusion. Orifice and capillary rheometry have been used to investigate the rheological properties of relatively concentrated suspensions (as opposed to rotational rheometers) [23], and helps establish the material shear stress and extrusion pressure dependence with respect to the applied shear rates (or velocities) [24,25].

The extrusion response of cement pastes and mortars has been shown to be dependent primarily on the extrusion geometry, the mode of extrusion (e.g., ram or screw), and the fresh material properties [21,26], as is the case with many concentrated suspensions. These characteristics also influence the print quality, and consequently the later-age properties of the printed components. For cementitious materials, the ram extrusion process through a barrel-die geometry is characterized mainly by the die-entry and die-landing pressures, the extrusion yield stress needed for the material to shape into the die, and the wall shear stress needed to overcome the frictional resistance in the die [13,27]. Thus, a combination of materials-and-process characteristics is needed to predict and control the print output. The controllable process characteristics include the extrusion geometry (e.g., barrel-to-die size ratio, angle of taper in the die), printer power, extrusion rate, and the print velocity, while the material-process synergy is reflected in the extrusion force-ram displacement relationships, from which several important parameters can be extracted[§]. The important parameters thus extracted are the steady-state pressure (a surrogate for extrusion yield stress) and its temporal evolution, and length of the dead-zone formed, which are useful in describing some of the material-process interactions [21]. Dead-zone is created due to the deposition of material in the barrel close to the die entry, which acts as a static zone causing disturbances in the flow paths, leading to poor extrudate quality [30,31]. The dead-zone builds up around the die entry as the material shears and flows radially in the vicinity while the generated zone acts like a conical die wall [26]. Dead-zone is generally a result of water filtration and consolidation effects, and is a function of material constitution and the ram velocity (which dictates the print velocity) [31,32]. Hence, the dead-zone length can be a useful, indirect indicator of the printability of the mixtures since a longer dead-zone invariably results in difficulties in extrusion, wastage of material, and inhomogeneous print quality [26]. Several experiments have shown that mixtures that demonstrate increased deadzone lengths in ram extrusion are found to be less amenable to screw extrusion printing also.

Although extrusion tests are used to characterize the material flow under pressure, the coupled effects of extrusion and 3D printing parameters that dictate the applicability of cementitious mixtures for 3D printing are not well described. This paper attempts to shed light primarily on the effects of print velocity on the ram extrusion characteristics of 3D printable cementitious binders, so as to determine the range of desirable print velocities for a given extruder geometry and printer properties. The influence of print velocity on extrusion pressure and dead-zone length, both of which needs to be optimized, necessitates the selection of

[§] While many of the commercial 3D printers are based on the principle of screw extrusion, there are several printers with piston pumps and controlled material feed systems that rely on ram extrusion [28]. Moreover, ram extrusion tests are more controllable and easily replicable in the laboratory, thus making it a valuable tool in characterizing the rheological parameters and establishing their linkage to the process parameters [29].

a desirable range of print velocities applicable for a material-geometry combination. The proposed approach can pave the way for an efficient test method for extrusion-based 3D printing, wherein material selection as well as printing process parameter selection (print velocity, in this case) can be accomplished based on steady-state pressure and dead-zone lengths determined from pressure-ram displacement relationships. A standardized paste ram extruder is relatively easy to fabricate, and thus, the tests can be carried out in typical concrete laboratories.

2 Experimental Program

This study pre-selects 3D printable binders to be used based on our previous work [27], so that the combined material-process parameters can be interrogated efficiently. A cylindrical barrel-die geometry is considered here, with a barrel-die entry diameter ratio of ~9 for extrusion. A range of print velocities are chosen such that the chosen materials are extruded continuously.

2.1 Materials and Mixtures

Ordinary Portland cement (OPC) conforming to ASTM C 150, micro silica (silica fume; M) conforming to ASTM C 1240, and fine limestone powder (L) conforming to ASTM C 568 were used to proportion the cementitious pastes used in this study. The chemical compositions of the starting materials are shown in

Table 1 and the paste constitutions in

Table 2. These paste mixtures were chosen based on previous study that showed that they are extrudable and printable [26]. The subscript numbers used in the mixture identifiers refer to the amount of OPC replaced by either microsilica or limestone, as a percentage of mass. The particle volume fractions and water-to-powder ratios (w/p) were varied based on the paste constituents used. The materials were dry-mixed for one to two minutes, followed by water addition and mixing at 1200 rpm for about three minutes. The mixtures with superplasticizers were mixed for three minutes at 1200 rpm, rested for one minute and mixed again for another minute. The prepared mixtures were used for rheological characterization, extrusion testing, and 3D printed into filaments and cubes. For extrusion testing and printing, the paste was filled in a cylindrical barrel of 100 mm length and a diameter of 35 mm (100 cm^3 volume). Care was taken to ensure that no air voids were entrapped during this process by tapping the filled geometry for about a minute to allow the air to move out.

Table 1: Chemical composition of the paste components

Components of the binder	Chemical composition (% by mass)						
	SiO_2	Al_2O_3	Fe_2O_3	CaO	MgO	SO_3	LOI
OPC	19.60	4.09	3.39	63.21	3.37	3.17	2.54
Microsilica	>90.0			<1.0			
Limestone ($1.5\mu m$)	$CaCO_3$ > 99%						

Table 2: Mixture proportions and relevant properties of the printable pastes

Mixture ID	Mass fraction of ingredients			Water-to-powder ratio (w/p) by mass	Super-plasticizer (% by mass of powder)	Particle volume fraction (Φ)
	OPC	Lime-stone (L); d_{50}=1.5	Micro-silica (M)			
L_{30}	0.70	0.30	0	0.41	0	0.324
L_{30}-s	0.70	0.30	0	0.35	0.25	0.382
$L_{15}M_{15}$	0.70	0.15	0.15	0.45	0	0.301

2.2 Rheological characterization

The mixture proportions were tested for yield stress and plastic viscosity using a parallel plate geometry on a TA Instruments AR2000ex rheometer. A 50 mm diameter serrated Peltier plate maintained at 25ºC was used. The gap between the top and bottom plates was kept at 5 mm. A logarithmic strain-rate sweep in the range of 0.1-100 s^{-1} was used to establish the shear stress-to-strain rate relationship [27,33]. The non-Newtonian mixtures are assumed to follow a power-law relationship and was fitted using:

$$\tau = k\dot{\gamma}^{n} \quad \text{Eq. 1}$$

where τ is the shear stress, $\dot{\gamma}$ is the shear rate, k is the fluid consistency index, and n is the flow index [34]. Note that relationships such as the Herschel-Bulkley model also can be used to fit the shear stress-strain rate relationship; the parameters k and n would slightly change in such a case, but the underlying trends remain unaffected.

2.3 3D printing

A customized BCN3D desktop paste printer shown in Figure 1a was used, along with the cylindrical barrel described above as the paste container. The cartesian printer has a print head that moves along the X-Z axis and the print stage moves along the Y-axis. The whole system is controlled by stepper motors (NEMA 17; 50 N-cm holding torque and gear train efficiency of 95%) programmed to generate linear motion, which controls the motion of the plunger and pushes the paste out of the nozzle as a function of the input print parameters (layer height and width, and print velocity). The customizable extruder fitted on the printer has a uniform nozzle with a die diameter of 4 mm. The die length is 36 mm and the barrel length where the material is initially placed is 100 mm as shown in Figure 1b. A thin layer of lubricant was applied before the paste was filled in the barrel to ensure easy and homogenous extrusion. The g-code generated using the Slic3r software, along with the print parameters (layer height, width, print speed and infill volume), were fed into the printer control unit. Filaments, 6 mm wide, 3 mm high, and 150 mm long (layer width and height taken as 1.5 and 0.75 times the nozzle diameter respectively) were printed as shown in Figure 1c. Figure 1d shows the hollow cubes printed using the chosen pastes, to ascertain shape stability. The extrusion rate is a function of motor speed, and a higher power is needed to extrude pastes of higher viscosity, for a

given extrusion geometry. The print velocity range was selected after carrying out printing at different speeds, ranging from 1 mm/s to 100 mm/s. It was observed that the chosen pastes failed to provide an acceptable print below a print speed of 5 mm/s (due to excessive liquid phase migration below a threshold velocity [35]) and above a print speed of 50 mm/s (due to motor stalling). Hence print speeds of 5, 15, 22.7, 35, and 50 mm/s were adopted for the selected pastes. Different print speeds are reported for gantry-based and robotic arm-based printing systems, based on the nozzle size and shape. However the higher range of speeds evaluated in this work conform to those reported in [36] for actual field-scale printing of mortars.

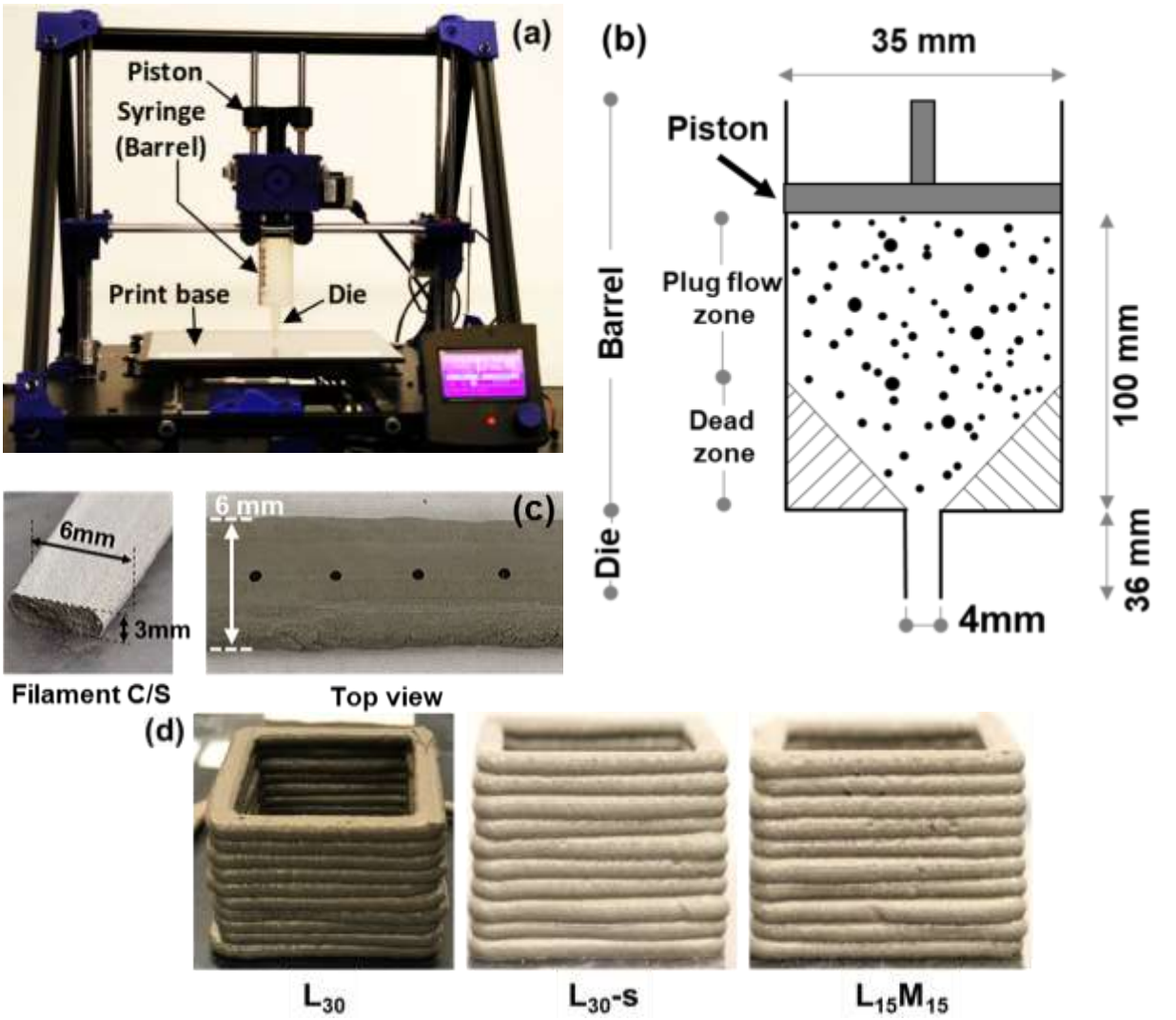

Figure 1: (a) 3D printer used for printing pastes, (b) extrusion barrel with a 4 mm diameter nozzle, (c) the filament dimensions used for printing, and (d) hollow cubes printed using L_{30}, L_{30}-s, and $L_{15}M_{15}$ pastes.

A measure of printability is arrived at in this study by printing a filament of aforementioned dimensions, and carefully measuring the layer height and layer width at different locations on the filament. Care was taken to reduce the volume- and/or shape-change (shrinkage) effects by preserving the specimens in

enclosed moist containers immediately after printing. After 24 hours, filaments were accurately measured for their heights and widths at every 10 mm spacing (black dots shown in Figure 1c). The printability is evaluated using a flow ratio (FR), defined as the ratio of measured-to-designed cross-sectional area of the printed filament [26]. The dimensional accuracy of the printed filament is quantified using FR. An improper material flow (both low and high) results in FR deviating from unity. Even though FR is an averaged quantity obtained from several individual dimensional quantifications, care was taken to ensure that the chosen filaments were dimensionally accurate, and that the standard deviations among the measurements made at different points along the filament were negligible, i.e., an FR close to unity is not obtained through averaging of values much higher and much lower than 1.0.

2.4 Extrusion characterization

The extrusion cell used in this study also employs the same cylindrical barrel used in the printer. The extruder barrel was filled with paste and agitated to remove entrapped air voids. The plunger was positioned coaxially in direct contact with the upper surface of the paste filled in the barrel. The extruder assembly was placed in a custom-fabricated holder (Figure 2a), and the top of the plunger pushed with the upper platen of a 4.45 kN MTS universal testing machine (UTM) operating in displacement-control mode at pre-defined velocities. The ram velocities required to obtain print velocities (or extrusion velocities) in the 5 to 50 mm/s range were obtained by equating the flow rates in the barrel and the flow rate corresponding to the printed element, i.e., $A_b V_{ram} = A_f V_p$, where A_b is the cross-sectional area of the cylindrical barrel, A_f is the cross-sectional area of the printed filament, and V_{ram} and V_p are the ram and print velocities respectively. Figure 2b shows the relationship between the ram velocity (the control parameter used in the tests) and the print velocity. The extrusion was stopped when the total ram displacement reached close to 100 mm, or when the pressure required to extrude the material caused noticeable changes in the extrudate quality. This was evident when a steep rise was noted in the force-ram displacement relationship. The extrusion pressure-ram displacement plots were analyzed to extract the steady-state pressure and dead-zone lengths as will be explained later.

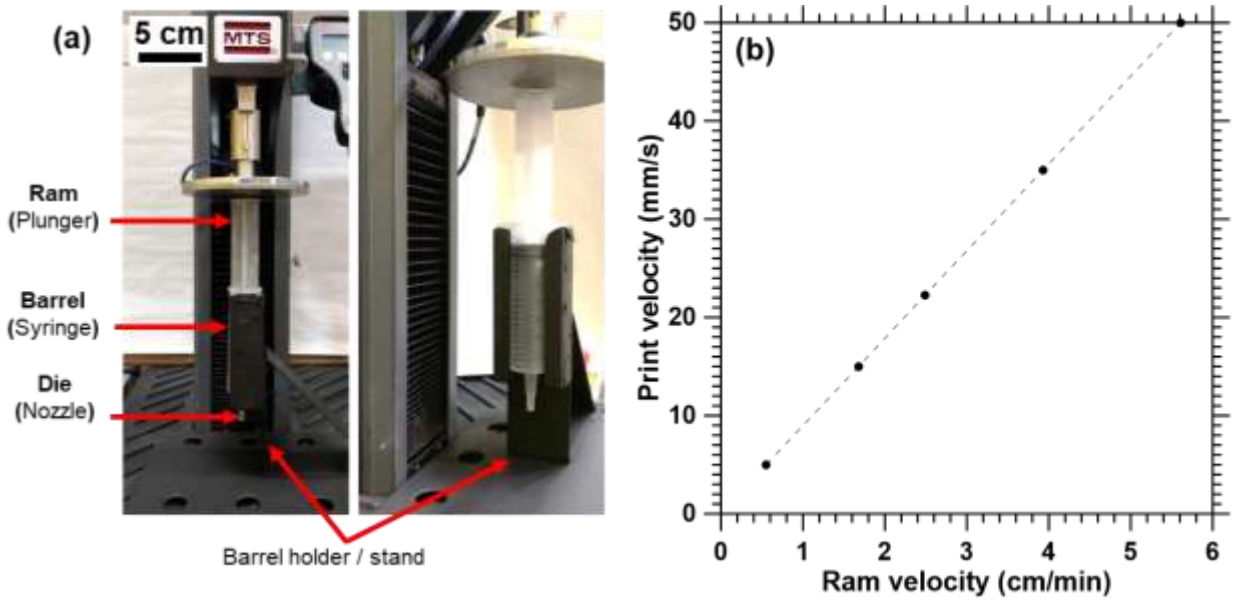

Figure 2: (a) Extrusion test setup and components, and (b) ram velocities and the equivalent print velocities used for extrusion and printing respectively.

2.5 Pressure drops during extrusion, and deposition pressure determination

The extrusion pressure is used to overcome the frictional and shaping stresses exerted on the material by the extrusion system to maintain the flow rate for the desired filament dimensions. Figure 3 shows the different pressure drops occurring during extrusion. The relationship between print speed and the maximum allowable filament height is established using the Hagen-Poiseuille equation, considering axisymmetric filament conditions (also called liquid bridge in fluid mechanics literature), given by [37]:

$$\frac{\pi d_{exit}^4 P_{outlet}}{8\eta L_{die} V_p} > \frac{h^2}{\pi} \qquad \text{Eq. 2}$$

where d_{exit} is the exit diameter of the nozzle, P_{outlet} is the pressure acting at the nozzle outlet, η is the viscosity, L_{die} is the length of the die, V_p is the print velocity, and h is the layer height. The maximum layer height for a given flow condition, beyond which the filament is unstable and slender, and would cause discontinuities for a given print velocity, can be extracted from Eq. 2. The axisymmetric bridge condition necessitates that the stretched filament (along the height) remains intact and does not break. Hence, the theoretical layer height based on axisymmetric bridging is rather unrealistic for cement pastes for the following reasons: (a) for soft materials such as cement pastes, longer bridge length results in filament buckling failure, and (b) the desired extrusion rate to satisfy this filament height is too high and invariably results in dimensional inaccuracies. A more realistic maximum layer height for 3D printed cementitious materials is based on the nozzle diameter used and reported in a companion study [38].

However, one needs to also determine a minimum layer height that can be printed under the given conditions, especially when the nozzle gets closer to the print surface, as explained later in this section. The total pressure of extrusion (P) is related to the resistance that the material experiences in the course of flow from the barrel until it exits the nozzle outlet, given as:

$$P = \Delta P_1 + \Delta P_2 + \Delta P_3 \quad \text{Eq. 3}$$

Here, the overall pressure drop during extrusion is generally divided into the pressure drops in the barrel (ΔP_1), die entry (ΔP_2), and die exit (ΔP_3). Several approaches have been used to estimate these pressures at different stages of extrusion. They include the phenomenological Benbow-Bridgewater model that divides the total pressure into the die entry and die-land pressures, and numerical simulations that consider constitutive relationships for modeling the process [13,16,21,39–41]. Recent work [42] has determined that when the nozzle is close to the print surface, there is an additional pressure drop between the die exit and the print surface (or the previously deposited material on which the layer is being printed) because the material has to flow through the gap between the nozzle and the print surface. This print deposition pressure (ΔP_4), which is a function of the print velocity, nozzle geometry, layer height, and the rheological characteristics of the paste can be estimated using Eq. 4, which is based on [42]:

$$\Delta P_4 = \left(\frac{min(w, D_{die})}{2} - \frac{d_{die}}{2}\right)\frac{k}{h^{1+n}}\left[\frac{(1+n)(1+2n)V_p}{n}\right]^n \quad \text{Eq. 4}$$

Here, w is the width of the filament, D_{die} is the outer diameter of the die, $min(w, D_{die})$ is the minimum value among w and D_{die}, d_{die} is the inner diameter of the die, V_p is the print velocity, and h is the filament height. The constants k and n are the consistency and flow indices of the material respectively, which can be determined using rheological tests as described earlier. This relationship can be used to define a minimum limit on the layer height for a given print velocity so that the pressure does not hinder deposition.

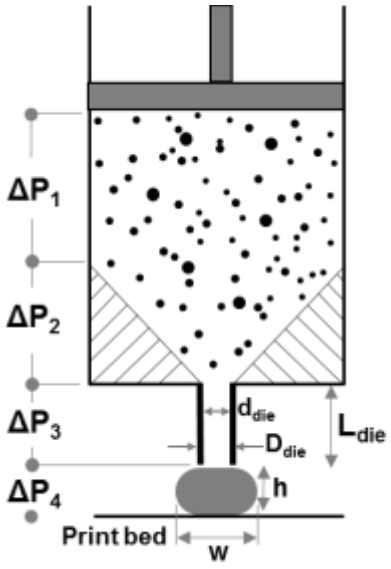

Figure 3: Schematic showing different pressure drops along the extruder and the parameters used in its estimation.

3 Results and Discussions

The cementitious mixtures used for printing should be both extrudable and printable. Extrudability refers to the ability of the mixture to homogenously extrude from the nozzle geometry under the required pressure, for a given print velocity. Printability refers to the shape stability of an individual filament, as well as layer stability when successive layers are stacked one above the other. This paper discusses extrudability using pressure-ram displacement relationships during extrusion and its analysis, and shape stability of an individual filament using the flow ratio.

3.1 Consistency and flow indices

The yield strength and plastic viscosity of the cementitious pastes determined using rotational shear rheometry are shown in Table 3. A vane shear yield stress greater than 150 Pa was found to result in adequate printability, as has been mentioned elsewhere also [27]. This corresponds to an extrusion yield stress of 200 kPa, which has been reported to be in the range suitable for extrusion, for similar materials [43]. The buildability of these pastes was tested by printing filaments 6 mm wide and 3 mm high, and stacked to at least 10 layers. Table 3 also shows the microstructural parameter for these pastes, defined as the ratio of their solid volume fraction and the square of the median particle size [44]. This factor has been shown to be highly correlated with rheological properties of importance in 3D printing [27]. The flow indices (n) of all the pastes are less than 1.0, denoting non-Newtonian behavior. The L_{30} paste has a relatively lower consistency index (k), indicating a more shear thinning response while the other two pastes have higher and similar k values, owing to combination of better packing and particle-particle interactions attributed to the presence of superplasticizer and/or finer particles (e.g., microsilica in the $L_{15}M_{15}$ paste).

The flow index is similar for the pastes containing superplasticizer or microsilica, indicating better print performance.

Table 3: Shear rheological parameters for the selected pastes

Mixture ID	Shear yield stress (τ_o)	Plastic viscosity (μ)	Microstructural parameter	Consistency index (k)	Flow index (n)
-	(Pa)	(Pa.s.)	(x 10^{-3} μm^{-2})	(Pa.s$^{1/n}$)	-
L_{30}	156	2.94	9.92	42.4	0.23
L_{30}-s	312.5	4.35	11.70	114	0.15
$L_{15}M_{15}$	191.3	2.71	13.83	94.9	0.15

3.2 Filament printing and flow ratio

Figure 4a shows the typical filaments of the L_{30} mixture printed at different speeds. It is observed that the filaments become narrower with increasing print speed. This is expected since the equivalence of flow rates (see Section 2.4) demands this. The filament dimensions were measured at discrete points as shown in Figure 4a to estimate the cross-sectional area and to subsequently calculate the flow ratio. Figure 4b shows the variation in flow ratio (FR) as a function of the print velocity for the different printable mixtures. This figure also includes the FR values of non-printable (too fluid or too stiff) mixtures (L_{30} mixture at higher and lower w/p ratios of 0.46 and 0.35 respectively; note that a w/p of 0.41 was used for the printable mixture) to show how the FR varies with print speed for non-printable mixtures. Also note that the results shown here are averaged values, from multiple points measured along multiple filaments printed. Slight changes in mixture composition and extrusion conditions result in dimensional variations, but the trends are found to be valid. It can be noticed that the flow ratios are very close to unity for the three printable mixtures. Thus it can be seen that, given the rheological characteristics of these printable mixtures, the printer allows for required paste flow to achieve the design dimensions. For highly flowable or stiff pastes, (e.g., vane shear yield stress lower than 150 Pa or higher than 600 Pa for a set of mixtures described in [45]), FR was found to significantly deviate from unity as shown in this figure, which is expected since in both the cases, it is difficult to maintain the shape – for the 0.46 w/p mixture, it is the instability resulting from a more fluid mixture, while for the 0.35 w/p mixture, it is discontinuity in extruded filaments because of higher pressures needed to extrude high yield stress suspensions [46]. Figure 4c shows the flow ratios of the printable mixtures alone as a function of the print speed. It can be noticed from this figure that, when the print velocity was increased beyond 22 mm/s, there was a drop in the flow ratio (based on the mixture type), resulting in thinner filaments being produced due to variations in the flow, similar to the results presented elsewhere [47]. This is because the required extrusion pressure approaches the maximum capacity of the printer for the selected speed. This is also a function of the rheology of the paste, influenced by its composition, particle sizes, *w/p* etc. [27,48]. However, for a given printer and chosen mixtures, optimal parameters can be arrived at, as discussed in later sections. In any case, FR can be used as a rather quick

method to examine the printability of different mixtures, though the authors do not recommend the use of FR as an absolute quantifier of printability.

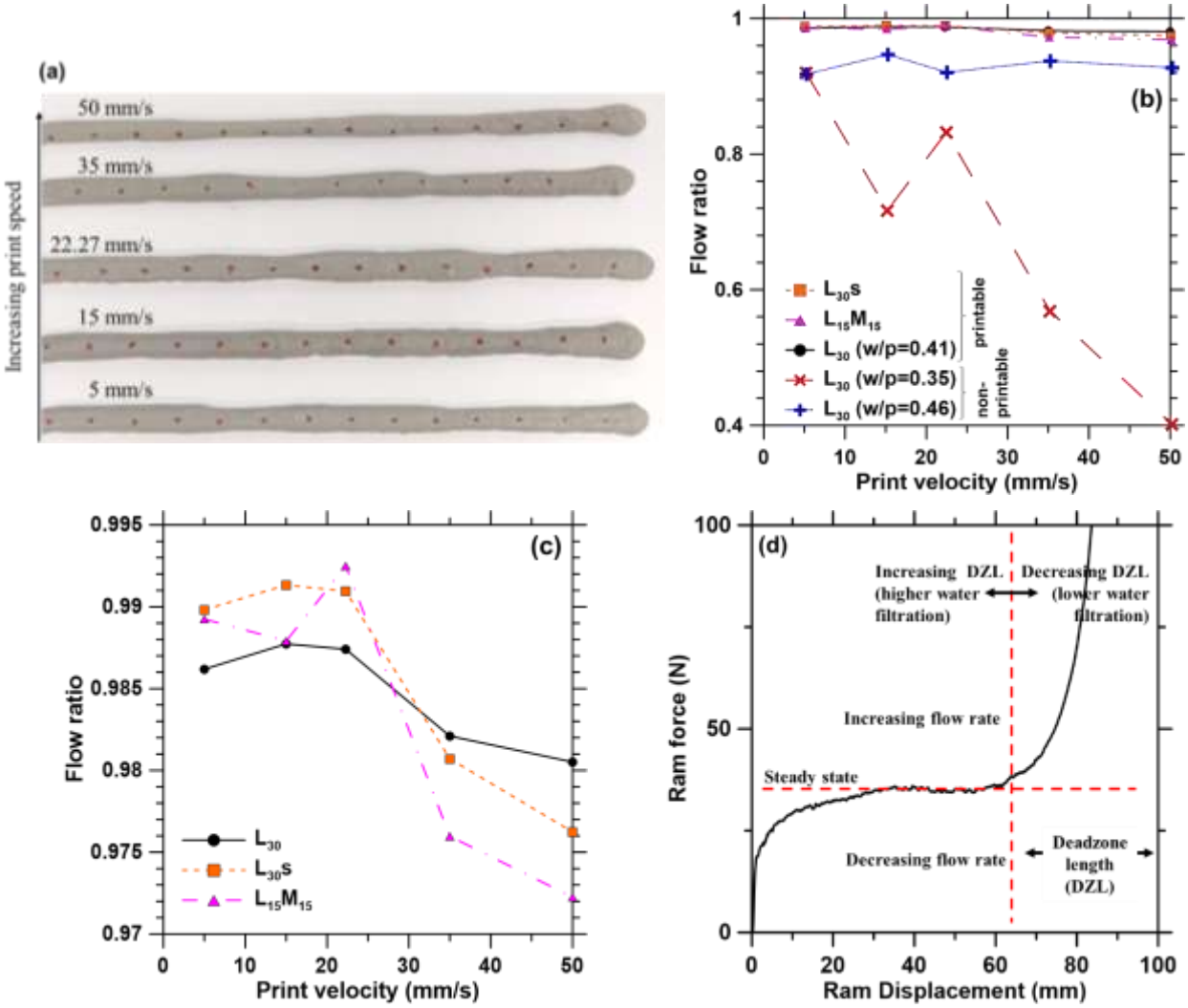

Figure 4: (a) Typical printed filaments of L_{30} paste used for flow measurements, at different print velocities, (b) flow ratio as a function of print velocity for printable (L_{30}s, $L_{15}M_{15}$, and L_{30} at w/p ratio of 0.41) and non-printable mixtures (L_{30} at w/p ratios of 0.35 and 0.46), (c) drop in the flow ratio of printable mixtures at higher velocities, and (d) typical force-ram displacement response under extrusion showing the steady state force and dead-zone length [26]. The standard deviations of flow ratio in (b) and (c) ranged from 0.015-0.025 for multiple dimensional measurements made at multiple points on 3-5 filaments for a given mixture at a certain print velocity, and are not explicitly shown to retain the readability of the graph. When a representative filament alone is considered, the standard deviations are lower.

3.3 Pressure-ram displacement response under extrusion

In order to correlate the print output to the characteristics that can be extracted from a standardizable test, extrusion tests at different print speeds were carried out by changing the ram velocity in the displacement-controlled loading test. Figure 4d shows a typical force-ram displacement plot showing the steady state

force and dead-zone length (DZL) for a given ram velocity. Note that the tests are carried out immediately after mixing, and thus the influence of time-dependent property evolution on extrusion characteristics are not considered here, and warrants a separate study. When the paste is pushed by the ram, there is a rapid increase in extrusion force (the very early rising portion in this curve) until the material yields and the paste extrudes through the die exit at a relatively constant pressure, referred to as the steady-state pressure (SSP). The steady-state pressure is an indicator of the stress required to shape the paste from the barrel to the die after pre-consolidation. Thus, this easily measurable value can be used as a proxy for the extrusion yield stress of the material when it just starts moving through the die entry. This value can be used in mixture characterization and qualification. Depending on the paste characteristics and the rate of loading (i.e., ram velocity), after a certain amount of material is pushed out, significantly higher force is required to extrude the paste. The point of rapid increase in force in the post-steady state flow condition, when the ram approaches the die entry, can be used to determine the residual material in the barrel that corresponds to a "dead-zone". It is reported that effects of paste consolidation and water filtration are responsible for dead-zone formation [31], which detrimentally influences the quality and uniformity of the extrudate. When the demand for flow rate increases due to increasing print speed or larger layer dimensions, it causes a steeper increase in the initial rising portion of the force-ram displacement relationship, as well as the steady state pressure. This is also likely to influence the dead-zone dimensions; a higher flow rate is found to generally result in a reduced dead-zone length in this work and similar observations are found elsewhere also [26]. A lower flow rate (i.e., smaller print velocity) could induce liquid phase filtration near the die entry, especially for concentrated suspensions such as cementitious binders used for 3D printing [21]. The binder is subjected to a higher stress gradient between the barrel and the die (also depends on the barrel-to-die diameter ratio), and hardening takes place due to filtration, thereby increasing the extrusion force. Both the steady-state pressure and the dead-zone length denoted in Figure 4d can be optimized for efficient extrusion. As a simple rule-of-thumb, extrusion pressure can be reduced by reducing the shear yield stress of the material, while the dead-zone length can be reduced by controlling the viscosity that restricts water filtration effects. However, a more-than-desired reduction in both these rheological parameters adversely impacts shape stability and buildability, necessitating the well-described need to carefully control mixture design for 3D printing.

The extrusion pressure-ram displacement response for the selected pastes at different print velocities are shown in Figure 5. The results discussed here are limited to one extrusion geometry with a uniform die of 4 mm diameter and a barrel-to-die diameter ratio of ~9. Our recent work has described the pressure-displacement response as a function of extruder geometry, emphasizing the influence of constrictivity between the barrel and the die on extrusion flow [26]. Maintaining the barrel-to-die diameter ratio relatively

constant ensures comparable trends in the extracted parameters, and hence the set up reported here can be expanded for use with mixtures containing larger sized particles (e.g., mortars) also. The steady-state pressure is observed to range between 25 and 40 kPa for the chosen pastes and the geometry (the geometry influences the steady-state pressure, and thus recommendation of the desired pressure range needs to consider the geometry) [26]; under this pressure, the chosen pastes are "firm" enough to ensure shape-stable extrusion, and "soft" enough to avoid excessive plastic deformation. The pressure required to extrude the material is found to increase with increasing print velocity. An increase in pressure at higher print velocities is attributed to the higher demand in the flow rate which requires the piston to apply more force to extrude the paste. This could be detrimental if the required pressure is close to, or exceeds the capacity of the printer, wherein discontinuous flow (broken filaments) will result, or the entire flow will cease. However, for a well-constituted paste, this is unlikely to be an issue when the printer system has stepper motors capable of imparting a holding torque of 50 N-cm (which translates to an upper limit of 50 kPa for the estimated equivalent extrusion stress, for the extruder used) as is commonly available with many commercial paste printers. A very low print velocity is generally observed to induce the formation of longer dead-zones, attributed to the magnified consolidation effects due to the slower application of force. At lower print velocities, the mixture with superplasticizer ($L_{30\text{-}S}$) demonstrates much lower SSPs as compared to the companion paste without superplasticizer (L_{30}). The higher particle concentration in the superplasticized mixture and the increased homogeneity ensures that particle reorganization occurs faster in the barrel and die, and smoother flow occurs with lesser effort initially, but gradual liquid phase filtration at the die entry causes the extrudate properties to change, resulting in a longer dead-zone. The SSPs for all the chosen mixtures at higher print velocities ($\geq$ 22.7 mm/s) are quite similar. One reason for this behavior is that, the stress distribution in the paste, the internal friction between particles, and the wall friction are rather constant under a faster extrusion process that does not provide ample time for particle reorganization and consequent liquid phase migration [32]. Thus, one potential indicator of critical print velocity is that velocity beyond which the steady state pressure shows minimal change. For different mixtures and printer characteristics, this can be easily determined using a simple displacement-controlled extrusion test.

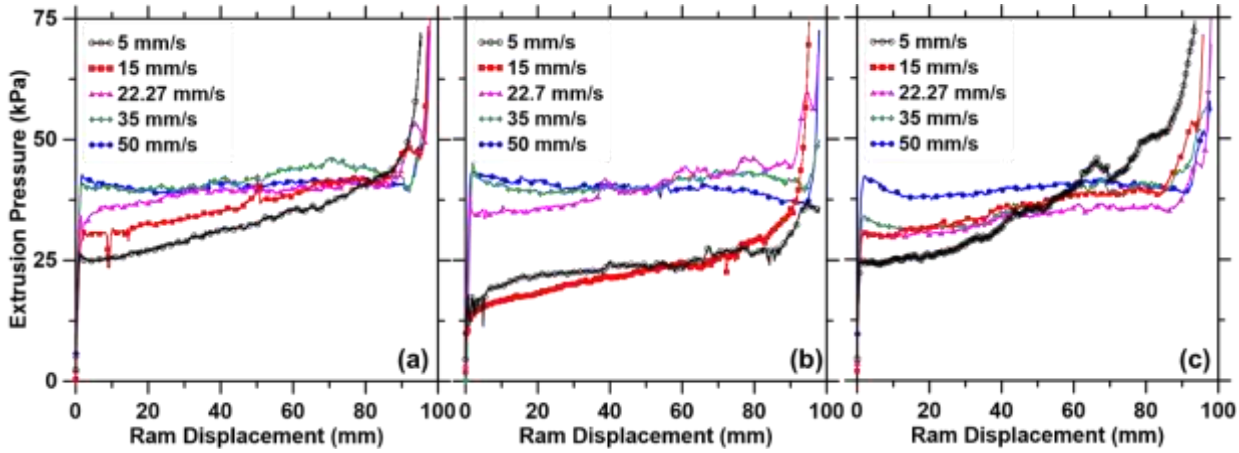

Figure 5: Extrusion pressure-ram displacement relationships at different print velocities for: (a) L_{30}, (b) L_{30}-s, and (c) $L_{15}M_{15}$ pastes. Representative plots are shown for each of the mixtures at a given print velocity. The standard deviation in the steady state pressures are generally less than 5 kPa for 3-5 replicate tests.

It is also instructive to note that even in the so-called SSP regime, there is sometimes a slight increase in pressure with ram displacement, especially for the pastes subjected to extrusion at low velocities. This translates into a faster rise at a lower ram displacement as compared to pastes extruded at higher velocities; in other words, a larger dead-zone length. At low print velocities, liquid phase migration (especially for concentrated suspensions) results in the extrudate containing more liquid than the initial mixture, and particle jamming occurring in the barrel. The material in the barrel becomes heterogeneous with consolidated material accumulating near the die entry (dead-zone; see Figure 1b). This results in an increase in internal shear and frictional stresses [49,50], thereby exponentially increasing the pressure required for extrusion (to greater than 50 kPa, for the pastes studied here) as noted at higher ram displacements (closer to the die entry) in Figure 5. This effect has been shown to be more prominent at higher barrel diameter-to-die entry ratios [15,26]. As can be easily understood, barrel-die constrictivity will enhance the pressure required for extrusion and consequently result in a longer deadzone. This aspect needs to be considered in the design of extrusion cell when used as a test method.

3.4 Velocity dependence of steady state pressure and dead-zone length

The print velocity dependence of SSP and dead-zone lengths are further elucidated in Figure 6. SSPs increase and the dead-zone lengths decrease as the print velocity increases, and there is a strong power-law dependence. The steady-state pressures and dead-zone lengths for these pastes at vanishing (very low) print velocities are the constants shown in the corresponding equations. The SSP values tend to show only minor changes beyond a print velocity of ~30 mm/s, and is in line with the flow ratios shown earlier. Figure 6a andFigure 6b show that the L_{30} paste results in somewhat higher extrusion pressure and dead-zone length as compared to the other pastes, for a chosen print velocity. The relationships between print velocity and

steady state pressure or dead-zone length are similar for the L_{30} and $L_{15}M_{15}$ pastes, attributable to the similarity in particle volume fractions, *w/p*, and the rheological characteristics of the pastes (see

Table 2). However, the $L_{15}M_{15}$ paste shows lower SSP and dead-zone lengths than the L_{30} paste at all print velocities. This could be attributed to the smaller particle sizes of silica fume that makes the mixture more cohesive, as well as improves the particle packing even when the overall solid volume fraction is slightly lower than that of the L_{30} paste (

Table 2). The $L_{15}M_{15}$ paste was determined to have a microstructural parameter [27] that is ~40% higher than that of the L_{30} paste (see Table 3). Better microstructural packing limits liquid phase migration, thereby reducing the pressure required for extrusion and the dead-zone lengths. The superplasticized paste (L_{30}S) shows lower SSP than the companion L_{30} paste at lower print velocities, but at higher velocities, the SSPs are virtually identical. One plausible reason for this could be the significantly higher slip layer thickness for the superplasticized mixture, quantified in our recent work [51]. The presence of superplasticizer enhances the slip velocity and reduces the wall shear stress for the same printing speed, thus resulting in a higher slip layer thickness. The reduction in dead-zone length of the L_{30}S paste as compared to that of the L_{30} paste can be attributed to improved microstructural packing (the microstructural parameter was 25% higher in this case as shown in Table 3). The foregoing discussion: (a) sheds light into the materials-related effects that dictate steady state pressure and dead-zone length as a function of print velocity, and (b) positions a simple ram-displacement controlled extrusion test as a viable means to evaluate the combined effects of materials- and printing-related parameters.

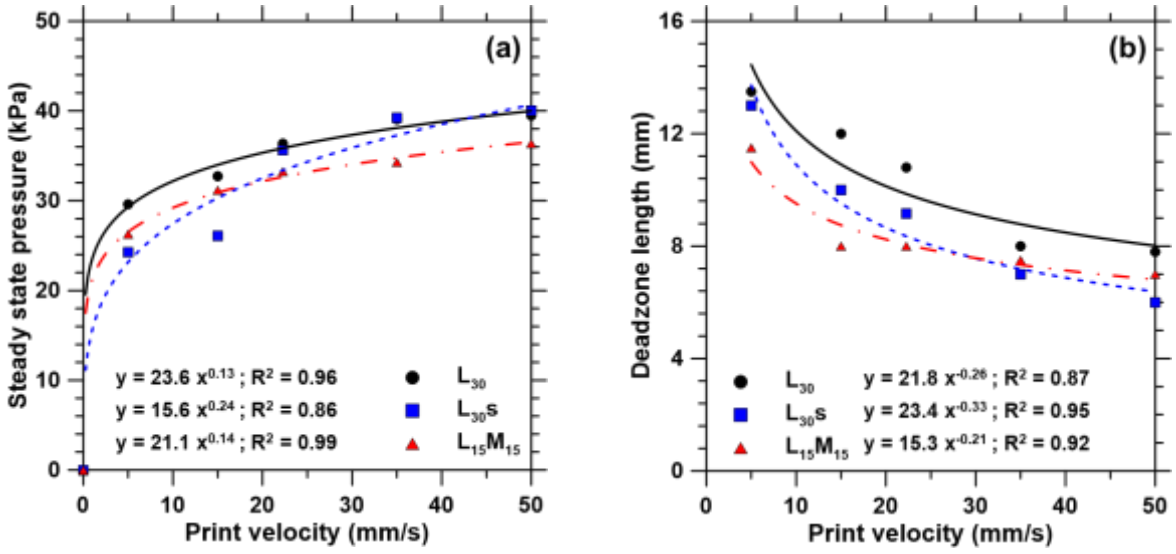

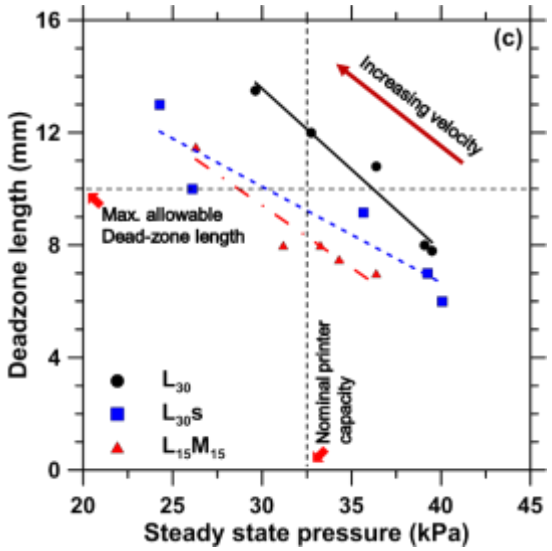

Figure 6: (a) Steady state pressure, and (b) dead-zone length dependence with print velocity, and (c) relationship between dead-zone length and steady state pressure. Each data point in (c), corresponding to a given mixture, relates to a certain print velocity.

Figure 6c shows that the dead-zone lengths are inversely related to the SSPs; essentially a conclusion that is arrived at from Figure 6a and Figure 6b. Based on this observation, it is plausible to determine an optimal velocity (or its range) which provides optimal values of SSP (less effort required for printing, thus having energy implications), and dead-zone lengths (implications on uniformity of the extrudate and material wastage). Based on a maximum allowable dead-zone length (corresponding to an extrudable paste) and a steady-state pressure that can be tolerated (based on the nominal capacity of the printer, as well as the characteristics of the mixture including its particle volume fraction and sizes), the DZL-SSP plot is divided into four quadrants. The maximum allowable dead-zone length and the steady-state pressure (based on printer capacity) are somewhat arbitrarily chosen here, but can be calibrated rather easily based on the binder materials that are under consideration and the process parameters. Data concentrated on the first quadrant (note that the absolute values shown are only as a guide to the eye) indicates a frictional and stiffer mix that requires higher extrusion pressure, for e.g., corresponding to the L_{30} paste in this case. Data in the third and fourth quadrants provide extrudate velocities where the dead-zone lengths are lower. Creating such plots for different mixtures and printing parameters using extrusion tests will aid in the identification and selection of print parameters and mixtures that optimize the desired output characteristics of the paste that are important in extrusion. This approach, hence, could lead to the standardization of a simple, but efficient qualification test method that employs easily definable extrusion process output parameters (SSP and DZL).

3.5 Effect of print deposition pressure on the extrudate quality

The consistency and flow indices (given in Table 3) are used in Eq. 4 to calculate the deposition pressure (ΔP_4) shown in Figure 7a. As the flow demand increases with increasing print velocity, the vertical force and the subsequent back pressure at the nozzle increases to cope up with required material deposition. While the paste will be extruded in this case, the demands on deposition rate at higher velocities cause discontinuities or flaws in the printed filament. When the extruder geometry and considered print velocities are the same, the deposition pressure is a function of the rheological properties of the paste, which is defined by the constants *k* and *m* in the rheological model described in Eq. 1. The deposition pressures determined using Eq. 4 are generally about half of the shear yield stress of the material, but significantly lower (by about 3 orders of magnitude) than the extrusional yield stress or the steady-state pressure. Moreover, the rate of change of deposition pressure with print velocity is seen to be independent of the paste composition, as shown in Figure 7a. The L_{30}s paste shows a relatively higher deposition pressure (60-80 Pa) likely due to a higher solids loading (the shear yield stress is also the highest for this mixture), while the L_{30} paste shows the lowest deposition pressure (20-40 Pa) and the lowest shear yield stress amongst the mixtures studied. It is interesting to note that although the SSPs (from Figure 6), especially in the lower range of print velocities, are generally lower for L_{30}s and $L_{15}M_{15}$ pastes than the L_{30} paste, the deposition pressures are higher for these pastes as shown in Figure 7b. This can be related to the higher consistency index (due to higher viscosity) or lower flow index (more non-Newtonian) of these pastes, suggesting that paste rheology acts as an indicator of the deposition pressure. The significant drop in flow ratio (dimensional accuracy), and increasing deposition pressure at higher velocities emphasize the need for an optimal range of print velocities where both the extrusion and print deposition processes are satisfactorily managed. The similar slopes of SSP vs. deposition pressure relationship for all the mixtures shown in Figure 7b demonstrate that the particle-scale mechanisms that control the SSP are responsible for the deposition pressure also, which once again, are deducible from a simple extrusion test.

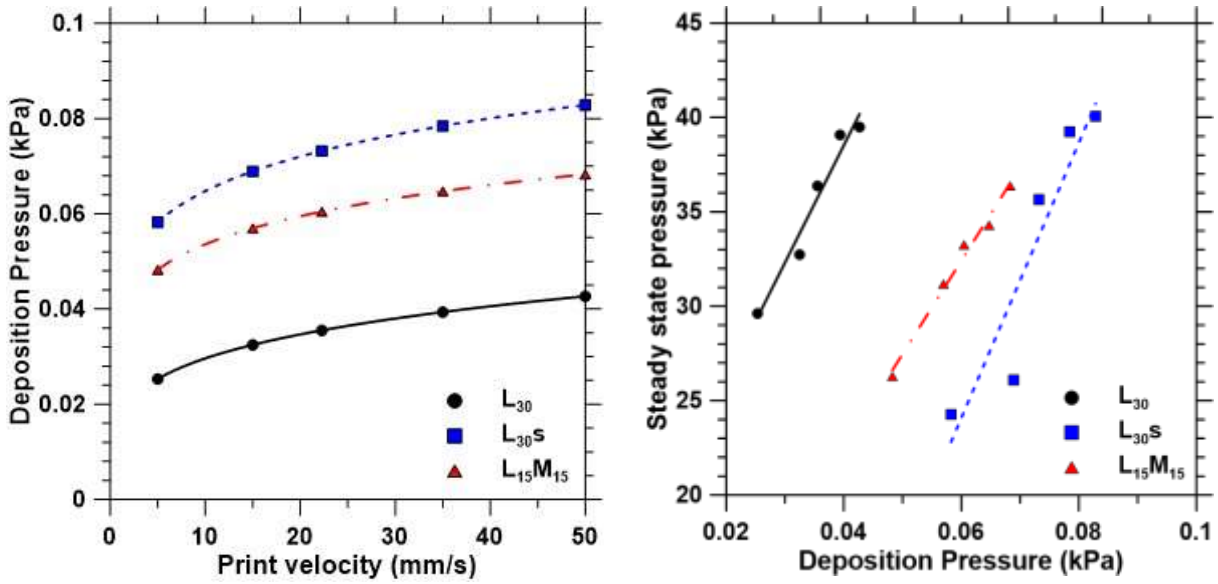

Figure 7: (a) The print velocity dependence of deposition pressure, and (b) the linear relationship between steady state pressure and the deposition pressure.

3.6 Desirable limits of velocity for print qualification

Based on the dependence of steady-state pressure, deposition pressure (which is directly related to SSP as shown in Figure 7b), and dead-zone length on print velocity, an optimal velocity can also be defined where the extrusion pressure is not too high for the printer, while keeping the dead-zone length minimal. Needless to say, this is a function of the printer type and capacity, mixture used for extrusion, and the geometry of the extruder. In fact, this corresponds to the velocity for the SSP-DZL combination that appears in the third quadrant of Figure 6c. To generalize this idea, Figure 8a shows the relationship between SSP and DZL with print velocity. A higher print velocity results in a higher steady state extrusion pressure, but at the same time, a lower dead-zone length. Although it is ideal to use a higher print velocity which could be beneficial in faster print rates and thus increased speed of construction, many other parameters, most important of them being buildability, needs to be considered for efficient 3D printing of concrete. For instance, very high printing speeds require the mixture to quickly gain sufficient strength before the next layer is printed. Any velocity exceeding a critical print velocity, defined here as that velocity beyond which the SSP exceeds the printer output limit, is impractical. This is the upper limit of print velocity for the chosen mixture-printer-extruder geometry combination. Similarly, the lower limit of desirable print velocity corresponds to a lower SSP that allows proper extrusion without the paste characteristics changing during the extrusion period because of liquid phase migration, i.e., this paste velocity results in tolerable lengths of the dead-zone. A smaller value for the lower limit of velocity opens up a larger range of acceptable print velocities for a given printer. This is advantageous since speeds may need to be lowered for finer printing needs (architectural shapes, special patterns etc.), critical paths in printing, or when the early strength development

is slightly delayed. The lower limit of desirable print velocities (based on Figure 8a) for the mixtures based on Figure 6a and Figure 6b, and the respective steady state pressures and dead zone lengths are shown in Figure 8b. Note that the limiting bounds for this graphical estimation are chosen as 50 kPa for SSP and 15 mm for DZL, based on user-defined system limits. It is to be noted that the lower limit of the desirable print velocities decreases (thereby enlarging the range of acceptable print velocities) with increase in the microstructural parameter (Table 3). Corresponding reductions are noticed in the steady-state pressure and dead-zone lengths as well. A better microstructural packing, through appropriate solid volume and selection of particle sizes, provides a wider range of acceptable print velocities. Since lower values of steady state pressure and dead-zone length, and a wider range of desirable velocities are advantageous for reasons explained earlier, compositional design of the paste can be achieved through the microstructural parameter, and the interaction between the selected mixture and the printing parameters can be quantified using the extrusion tests and corresponding analysis presented in this paper.

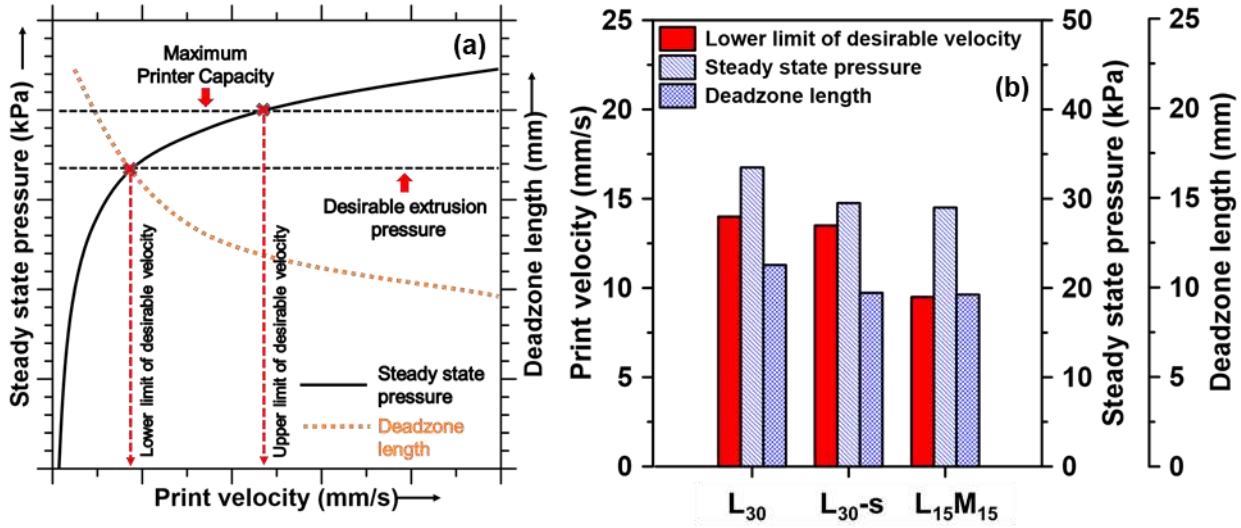

Figure 8: (a) Steady state pressure and dead-zone length as a function of print velocity to delineate the desirable range of print velocities, and (b) comparison of lower limit of desirable velocity, and its corresponding steady state pressure and dead-zone lengths for the selected mixtures.

4 Conclusions

This paper has discussed the extrusion process characteristics and quality of the print output, evaluated on three 3D printable cementitious binders, to suggest desirable limits of print velocity, steady state extrusion pressure, and dead-zone lengths. The results and recommendations rely on the capacity of the printer and the extruder geometry, and provides the fundamental understanding needed to develop a potential test method for mixture and process qualification using ram extrusion. The print output was characterized using a flow ratio based on filament dimensions, which showed that there exists a desirable velocity range beyond which the print output quality deteriorates. While this was primarily attributed to the capacity of the printer,

the mixture characteristics also influence this response. Extrusion tests were used to extract the steady state pressures and dead-zone lengths in the range of print velocities used. Steady state pressures were found to be directly related to the print velocities while dead-zone lengths were inversely related. The deposition pressure, which is a function of the rheological properties of the paste and the print velocity, guides the minimum height of the printed filament, and hence it is of importance in extrusion printing. The deposition pressure was also closely related to the steady state pressure (and yield stress) of the pastes. The steady state pressures and dead-zone lengths were used to arrive at desirable print velocities for a given binder and the printing system, to ensure that the printing process and the extrudate quality were within acceptable limits. This was accomplished by using the print velocity corresponding to the printer capacity (or close to it) as the upper limit for desirable velocity, and a velocity that minimizes the dead-zone length to a tolerable value as its lower limit. The time-dependent property evolution of the mixture also needs to be considered in the determination of upper velocity limit since fast printing rates on a softer material causes early failure. Since low velocities were found to result in larger dead-zone lengths due to liquid phase migration, achieving a lower limit of desirable print velocity that is small enough extends the acceptable range of print velocities. The lower limit also corresponds to a lower steady-state extrusion pressure, i.e., reduced effort resulting in reduced energy demand. The larger the acceptable range of print velocities for a binder, the more robust it is for 3D printing. Within the scope of the binders used, it was also found that a better paste microstructural packing, through particle size distribution and volume fraction, provides a wider range of acceptable print velocities. Thus, a combination of better material design and knowledge of print velocity-extrusion characteristics (steady-state pressure and dead-zone length) provides for improved efficiency in 3D printing of cementitious binders. The proposed approach can be synthesized in the form of a test method for paste and process qualification.

5 Acknowledgments

The authors sincerely acknowledge support from U.S. National Science Foundation (CMMI: 1727445; OISE: 2020095) towards this project. The authors also acknowledge the support from Salt River Materials Group, Omya, and BASF in donating the materials. We acknowledge the use of 3D printing and material characterization facilities within Laboratory for the Science of Sustainable Infrastructural Materials (LS-SIM) at Arizona State University.

6 References

[1] T.A.M. Salet, Z.Y. Ahmed, F.P. Bos, H.L.M. Laagland, Design of a 3D printed concrete bridge by testing, Virtual Phys. Prototyp. 13 (2018) 222–236. https://doi.org/10.1080/17452759.2018.1476064.

[2] G. Vantyghem, W. De Corte, E. Shakour, O. Amir, 3D printing of a post-tensioned concrete girder designed by topology optimization, Autom. Constr. 112 (2020) 103084. https://doi.org/10.1016/j.autcon.2020.103084.

[3] T. Wangler, E. Lloret, L. Reiter, N. Hack, F. Gramazio, M. Kohler, M. Bernhard, B. Dillenburger, J. Buchli, N. Roussel, Digital concrete: opportunities and challenges, RILEM Tech. Lett. 1 (2016) 67–75.
[4] B. Panda, C. Unluer, M.J. Tan, Extrusion and rheology characterization of geopolymer nanocomposites used in 3D printing, Compos. Part B Eng. 176 (2019) 107290. https://doi.org/10.1016/j.compositesb.2019.107290.
[5] V. Mechtcherine, V.N. Nerella, F. Will, M. Näther, J. Otto, M. Krause, Large-scale digital concrete construction – CONPrint3D concept for on-site, monolithic 3D-printing, Autom. Constr. 107 (2019) 102933. https://doi.org/10.1016/j.autcon.2019.102933.
[6] M.K. Mohan, A.V. Rahul, G. De Schutter, K. Van Tittelboom, Extrusion-based concrete 3D printing from a material perspective: A state-of-the-art review, Cem. Concr. Compos. 115 (2021) 103855. https://doi.org/10.1016/j.cemconcomp.2020.103855.
[7] B. Lu, Y. Weng, M. Li, Y. Qian, K.F. Leong, M.J. Tan, S. Qian, A systematical review of 3D printable cementitious materials, Constr. Build. Mater. 207 (2019) 477–490. https://doi.org/10.1016/j.conbuildmat.2019.02.144.
[8] G. Ma, L. Wang, A critical review of preparation design and workability measurement of concrete material for largescale 3D printing, Front. Struct. Civ. Eng. 12 (2018) 382–400. https://doi.org/10.1007/s11709-017-0430-x.
[9] S.R. Abid, K. Al-lami, Critical review of strength and durability of concrete beams externally bonded with FRP, Cogent Eng. 5 (2018) 1525015. https://doi.org/10.1080/23311916.2018.1525015.
[10] W. GleiE, Rheological Investigation of Suspensions and Ceramic Pastes: Characterization of Extrusion Properties t, (1993) 13.
[11] Z.D. Jastrzebski, Entrance Effects and Wall Effects in an Extrusion Rheometer during Flow of Concentrated Suspensions, Ind. Eng. Chem. Fundam. 6 (1967) 445–454. https://doi.org/10.1021/i160023a019.
[12] E. Bagley, End corrections in the capillary flow of polyethylene, J. Appl. Phys. 28 (1957) 624–627.
[13] J.J. Benbow, S.H. Jazayeri, J. Bridgwater, The flow of pastes through dies of complicated geometry, Powder Technol. 65 (1991) 393–401.
[14] Burbidge AS, Bridgwater J, Saracevic Z, Liquid Migration in Paste Extrusion, Chem. Eng. Res. Des. 73 (1995) 810–816.
[15] M. Bayfield, J.A. Haggett, M.J. Williamson, D.I. Wilson, A. Zargar, Liquid Phase Migration in the Extrusion of Icing Sugar Pastes, Food Bioprod. Process. 76 (1998) 39–46. https://doi.org/10.1205/096030898531738.
[16] S.L. Rough, D.I. Wilson, J. Bridgwater, A model describing liquid phase migration within an extruding microcrystalline cellulose paste, Chem. Eng. Res. Des. 80 (2002) 701–714.
[17] W.Z. Misiolek, Material physical response in the extrusion process, J. Mater. Process. Technol. 60 (1996) 117–124. https://doi.org/10.1016/0924-0136(96)02316-3.
[18] A. Perrot, Y. Mélinge, P. Estellé, C. Lanos, Vibro-extrusion: a new forming process for cement-based materials, Adv. Cem. Res. 21 (2009) 125–133. https://doi.org/10.1680/adcr.2008.00030.
[19] J.-Z. Liang, Influence of die angles on pressure drop during extrusion of rubber compound, J. Appl. Polym. Sci. 80 (2001) 1150–1154. https://doi.org/10.1002/app.1198.
[20] I. Aydin, F.R. Biglari, B.J. Briscoe, C.J. Lawrence, M.J. Adams, Physical and numerical modelling of ram extrusion of paste materials: conical die entry case, Comput. Mater. Sci. 18 (2000) 141–155.
[21] A. Perrot, D. Rangeard, Y. Melinge, P. Estelle, C. Lanos, Extrusion Criterion for Firm Cement-based Materials, Appl. Rheol. 19 (2009). https://doi.org/10.3933/ApplRheol-19-53042.
[22] P.D. PATIL, Modeling and Flow Simulation of Polytetrafluoroethylene (PTFE) Paste Extrusion, (n.d.) 144.
[23] A.U. Khan, N. Mahmood, A.A. Bazmi, Direct comparison between rotational and extrusion rheometers, in: 2009. https://doi.org/10.1590/s1516-14392009000400017.

[24] R.A. Basterfield, C.J. Lawrence, M.J. Adams, On the interpretation of orifice extrusion data for viscoplastic materials, Chem. Eng. Sci. 60 (2005) 2599–2607.
[25] P.J. Martin, D.I. Wilson, A critical assessment of the Jastrzebski interface condition for the capillary flow of pastes, foams and polymers, Chem. Eng. Sci. 60 (2005) 493–502. https://doi.org/10.1016/j.ces.2004.08.011.
[26] S.A.O. Nair, S. Panda, M. Santhanam, G. Sant, N. Neithalath, A critical examination of the influence of material characteristics and extruder geometry on 3D printing of cementitious binders, Cem. Concr. Compos. 112 (2020) 103671. https://doi.org/10.1016/j.cemconcomp.2020.103671.
[27] S.A. Nair, H. Alghamdi, A. Arora, I. Mehdipour, G. Sant, N. Neithalath, Linking fresh paste microstructure, rheology and extrusion characteristics of cementitious binders for 3D printing, J. Am. Ceram. Soc. 102 (2019) 3951–3964.
[28] G. Ji, T. Ding, J. Xiao, S. Du, J. Li, Z. Duan, A 3D Printed Ready-Mixed Concrete Power Distribution Substation: Materials and Construction Technology, Materials. 12 (2019) 1540. https://doi.org/10.3390/ma12091540.
[29] A. Perrot, D. Rangeard, V. Nerella, V. Mechtcherine, Extrusion of cement-based materials - an overview, RILEM Tech. Lett. 3 (2019) 91–97. https://doi.org/10.21809/rilemtechlett.2018.75.
[30] S. Alexandrov, G. Mishuris, W. Miszuris, R.E. Sliwa, On the dead-zone formation and limit analysis in axially symmetric extrusion, Int. J. Mech. Sci. 43 (2001) 367–379. https://doi.org/10.1016/S0020-7403(00)00016-3.
[31] A. Perrot, C. Lanos, Y. Melinge, P. Estellé, Mortar physical properties evolution in extrusion flow, Rheol. Acta. 46 (2007) 1065–1073. https://doi.org/10.1007/s00397-007-0195-6.
[32] H. Khelifi, A. Perrot, T. Lecompte, D. Rangeard, G. Ausias, Prediction of extrusion load and liquid phase filtration during ram extrusion of high solid volume fraction pastes, Powder Technol. 249 (2013) 258–268. https://doi.org/10.1016/j.powtec.2013.08.023.
[33] K. Vance, G. Sant, N. Neithalath, The rheology of cementitious suspensions: A closer look at experimental parameters and property determination using common rheological models, Cem. Concr. Compos. 59 (2015) 38–48. https://doi.org/10.1016/j.cemconcomp.2015.03.001.
[34] R. Shaughnessy, P.E. Clark, The rheological behavior of fresh cement pastes, Cem. Concr. Res. 18 (1988) 327–341. https://doi.org/10.1016/0008-8846(88)90067-1.
[35] H. Liu, J. Liu, M.C. Leu, R. Landers, T. Huang, Factors influencing paste extrusion pressure and liquid content of extrudate in freeze-form extrusion fabrication, Int. J. Adv. Manuf. Technol. 67 (2013) 899–906. https://doi.org/10.1007/s00170-012-4534-0.
[36] R.A. Buswell, W.R. Leal de Silva, S.Z. Jones, J. Dirrenberger, 3D printing using concrete extrusion: A roadmap for research, Cem. Concr. Res. 112 (2018) 37–49. https://doi.org/10.1016/j.cemconres.2018.05.006.
[37] R.S. Crockett, P.D. Calvert, The Liquid-To-Solid Transition in Stereodeposition Techniques, (n.d.) 8.
[38] S.A.O. Nair, A. Tripathi, N. Neithalath, Examining layer height effects on the flexural and fracture response of plain and fiber-reinforced 3D-printed beams, (2020).
[39] M. Li, L. Tang, R.G. Landers, M.C. Leu, Extrusion Process Modeling for Aqueous-Based Ceramic Pastes—Part 1: Constitutive Model, J. Manuf. Sci. Eng. 135 (2013) 051008-051008–7. https://doi.org/10.1115/1.4025014.
[40] M.J. Patel, S. Blackburn, D.I. Wilson, Modelling of paste ram extrusion subject to liquid phase migration and wall friction, Chem. Eng. Sci. 172 (2017) 487–502. https://doi.org/10.1016/j.ces.2017.07.001.
[41] X. Zhou, Z. Li, Numerical simulation of ram extrusion in short-fiber-reinforced fresh cementitious composites, J Mech Mater Struct. 4 (2009) 1755–1769.
[42] G. Percoco, L. Arleo, G. Stano, F. Bottiglione, Analytical model to predict the extrusion force as a function of the layer height, in extrusion based 3D printing, Addit. Manuf. 38 (2021) 101791. https://doi.org/10.1016/j.addma.2020.101791.

[43] P.F.G. Banfill, Rheology of fresh cement and concrete, Rheol. Rev. 2006 (2006) 61.
[44] R.J. Flatt, P. Bowen, Yodel: A Yield Stress Model for Suspensions, J. Am. Ceram. Soc. 89 (2006) 1244–1256. https://doi.org/10.1111/j.1551-2916.2005.00888.x.
[45] H. Alghamdi, S.A.O. Nair, N. Neithalath, Insights into material design, extrusion rheology, and properties of 3D-printable alkali-activated fly ash-based binders, Mater. Des. 167 (2019) 107634. https://doi.org/10.1016/j.matdes.2019.107634.
[46] Y. Chen, S. Chaves Figueiredo, Ç. Yalçinkaya, O. Çopuroğlu, F. Veer, E. Schlangen, The Effect of Viscosity-Modifying Admixture on the Extrudability of Limestone and Calcined Clay-Based Cementitious Material for Extrusion-Based 3D Concrete Printing, Materials. 12 (2019) 1374. https://doi.org/10.3390/ma12091374.
[47] Y.W.D. Tay, M.Y. Li, M.J. Tan, Effect of printing parameters in 3D concrete printing: Printing region and support structures, J. Mater. Process. Technol. 271 (2019) 261–270. https://doi.org/10.1016/j.jmatprotec.2019.04.007.
[48] N. Roussel, Rheological requirements for printable concretes, Cem. Concr. Res. 112 (2018) 76–85. https://doi.org/10.1016/j.cemconres.2018.04.005.
[49] T. Lecompte, A. Perrot, V. Picandet, H. Bellegou, S. Amziane, Cement-based mixes: Shearing properties and pore pressure, Cem. Concr. Res. 42 (2012) 139–147. https://doi.org/10.1016/j.cemconres.2011.09.007.
[50] J. Yammine, M. Chaouche, M. Guerinet, M. Moranville, N. Roussel, From ordinary rhelogy concrete to self compacting concrete: A transition between frictional and hydrodynamic interactions, Cem. Concr. Res. 38 (2008) 890–896. https://doi.org/10.1016/j.cemconres.2008.03.011.
[51] S.A.O. Nair, N. Neithalath, Flow Characterization of 3D Printable Cementitious Pastes during Extrusion using Capillary Rheometry, accepted for publication in ACI Mat. J.